J Mol Model (2011) 17:173–179
DOI 10.1007/s00894-010-0691-y

ORIGINAL PAPER

Optimal molecular structures of prion AGAAAAGA amyloid fibrils formatted by simulated annealing

Jiapu Zhang

Received: 10 November 2009 / Accepted: 11 February 2010 / Published online: 22 April 2010

Abstract To date, there is little structural data available on the AGAAAAGA palindrome in the hydrophobic region (113–120) of prion proteins, although many experimental studies have shown that this region has amyloid fibril forming properties. This region belongs to the N-terminal unstructured region (1–123) of prions, the structure of which has proved hard to determine using NMR or X-ray crystallography. This paper reports the successful construction of three amyloid fibril models for this region. The models were formatted by standard simulated annealing using suitable templates from the Protein Data Bank, and were refined using several traditional optimization methods within AMBER. Because the NMR or X-ray structure of the hydrophobic region AGAAAAGA of prion proteins has not yet been determined, these models can be used as a reference for experimental studies on this region. The results presented here confirm standard simulated annealing as an effective tool in molecular modeling. The three constructed models for amyloid fibrils may be useful in furthering the goals of medicinal chemistry in this field.

Keywords Molecular modeling · Prion palindrome · Amyloid fibrils · Simulated annealing · Optimization

Introduction

Prion diseases are invariably fatal and highly infectious neurodegenerative diseases that affect humans and animals. These neurodegenerative diseases are caused by conversion of the prion protein (PrP) from a soluble into an insoluble fibrillar form [1, 2]. The infectious prion (PrP^{Sc}) is an abnormally folded form of the normal cellular prion (PrP^{C}) [1–3]. The conversion of PrP^{C} to PrP^{Sc} is believed to involve a conformational change from a predominantly α-helical protein (42% α-helix, 3% β-sheet) to a protein rich in β-sheets (30% α-helix, 43% β-sheet) [3]. Prion amyloid fibrils are believed to be rich in β-sheet structure and to contain a cross-β core. Many experimental studies [e.g. 4–11] have shown that the hydrophobic region AGAAAAGA of prion proteins (113–120) plays an important role in the conversion of PrP^{C} to PrP^{Sc}. PrP lacking, or deleted in, the palindrome (PrP 113–120) neither convert to PrP^{Sc} nor generate proteinase K-resistant PrP [5, 6, 10, 11]. Brown et al. [4, 12] pointed out that the AGAAAAGA peptide was necessary, but not sufficient, for blocking the toxicity and amyloidogenicity of PrP 106–126. The peptide AGAA did not form fibrils but the peptide AGAAAAGA formed fibrils in both water and phosphate-buffered saline (PBS) [4]. Thus, the minimum sequence necessary for fibril formation should be AGAAA, AAAGA, AGAAAA, GAAAAG, AAAAGA, AGAAAAG, GAAAAGA or AGAAAAGA (in this paper AGAAAA, AGAAAAG and GAAAAGA will be used). According to Brown [4], AGAAAAGA is important for fibril formation and is an inhibitor of PrP^{Sc} neurotoxicity. Studies on atomic-resolution structures of the AGAAAAGA peptide will be useful to further the goals of medicinal chemistry for controlling prion diseases. The motivation of this paper was to study the atomic-resolution structures of the AGAAAAGA peptide of prions.

Many other experimental studies [e.g. 7, 9] have also shown that the hydrophobic region AGAAAAGA of prion proteins (113–120) has amyloid fibril forming properties. However, to date, little structural data for this region exists.

J. Zhang (✉)
Victorian Life Sciences Computation Initiative,
The University of Melbourne,
1–3 Hull Road,
Croydon, Victoria VIC 3136, Australia
e-mail: jiapu_zhang@hotmail.com

It is well known that the N-terminal residues (1–123) of prion proteins are unstructured, and the AGAAAAGA (113–120) region falls just within this region; NMR and X-ray crystallography cannot easily determine the molecular structure of the N-terminal region despite the fact that properties of the stability of prion proteins might be attributable mainly to the N-terminal unstructured region [13]. Due to the noncrystalline and insoluble nature of the amyloid fibril, it is difficult to obtain atomic-resolution structures using traditional experimental methods.

Computational approaches, however, allow us to obtain a description of the peptide at a submicroscopic level. This paper reports the computational construction of some amyloid fibril models for the hydrophobic region AGAAAAGA palindrome of prion proteins (113–120) that should prove useful in future experimental studies on this region. Aspects of the structure or the dynamics of the AGAAAAGA region should play a role in the aggregation process, and knowledge of these may be useful for the goals of medicinal chemistry for controlling prion diseases. Some previous studies on prions have focused on the PrP 106–126 region [7–9, 14–18]. After the breakthrough work of Sawaya et al. in 2007 [19], many computational studies have been done on prion or yeast prion amyloid fibrils [20–25]; this paper presents a computational study of the PrP 113–120 region of PrP 106–126.

Materials and methods

Recently, common structural features shared by all amyloid fibrils were revealed by Sawaya et al. [19]; the atomic structures of all the microcrystals examined revealed steric zippers, with strong van der Waals interactions between β-sheets and hydrogen bonds to maintain the β-strands. Based on these steric zippers, three prion AGAAAAGA palindrome amyloid fibril models will be constructed. Model 1 belongs to Class 7 of Sawaya et al. [19], Models 2–3 belong to Class 1 of Sawaya et al. [19] (in the author's experience, for prion AGAAAAGA palindrome, the β-sheet structure of other Classes proposed by Sawaya et al. [19] cannot be preserved after optimizations or simulated annealing).

The models were built on the LYQLEN peptide derived from human insulin residues 13–18 (PDB entry 2OMP [19, 26]) and the GNNQQNY peptide from the yeast prion protein Sup35 (PDB entry 1YJP [19, 26]). A 12-chain AGAAAA model (Model 1), a 10-chain AGAAAAG model (Model 2), and a 10-chain GAAAAGA model (Model 3) were successfully constructed. Models were separately constructed by the unmerge, mutate, and merge modules of Insight II (http://accelrys.com/). Model 1 (with EFABIJ LKDCHG chains) was derived from 2OMP.pdb; its AB chains were simply obtained from the AB chains of 2OMP.pdb by the unmerge, mutate and merge modules of Insight II, and the remaining chains were obtained using the mathematical formulas C=A+(−1.885 0 17.243), D=B+(−1.885 0 17.243), I=A+(9.666 0 0), J=B+(9.666 0 0), E=A+(−9.666 0 0), F=B+(−9.666 0 0), H=D+(9.666 0 0), G=C+(9.666 0 0), L=D+(−9.666 0 0), K=C+(−9.666 0 0). The B chain of 1YJP.pdb can then be obtained by the mathematical formula

$$B = \begin{pmatrix} -1 & 0 & 0 \\ 0 & 1 & 0 \\ 0 & 0 & -1 \end{pmatrix} A + \begin{pmatrix} 0 \\ 2.433 \\ 0 \end{pmatrix} \quad (1)$$

from its A chain. AB chains of Models 2–3 were constructed separately from the AB chains of 1YJP.pdb using the unmerge, mutate, and merge modules of Insight II; other chains of Models 2–3 were obtained from AB chains by parallelization of the AB chains. The initial structures of Models 1–3 are shown in Fig. 1.

The models were firstly optimized by the steepest descent (SD) and conjugate gradient (CG) methods [27–30]. These two methods are traditional optimization methods. The former has nice convergence but is slow when close to minimums. The latter is efficient but its gradient RMS and GMAX gradient [27–30] do not have a good convergence. We used the SD method followed by the CG method to optimize our models. When the models could not be optimized further, we employed standard simulated annealing (SA) [27, 31, 32]. The numerical potential energy results showed that SA is very effective for further optimizations and models 1–3 reported in this paper should be very useful to study the hydrophobic region AGAAAAGA palindrome of prion proteins (113–120). To summarize, the models were optimized by SD and CG methods, formatted by SA and finally refined using SD and CG methods. The work was performed with the AMBER 10 package [27] and the graphs were drawn with XMGRACE of Grace 5.1.21 and VMD 1.8.7beta5 [33].

We used the ff03 force field of the AMBER 10 package, in a neutral pH environment. The systems were surrounded with a 12 Å layer of TIP3PBOX water molecules using the XLEaP module of AMBER 10.

The solvated proteins were minimized by the SD method and then CG was performed. Model 1 was optimized by 57,350 steps of SD and 26,784 steps of CG; Model 2 by 57,950 steps of SD and 23,943 steps of CG; and Model 3 by 59,500 steps of SD and 23,109 steps of CG.

The solvated proteins were then quickly heated from 0 K to 300 K linearly for 20 ps. The systems were kept at 300 K for 80 ps. The systems then were slowly cooled from 300 K to 100 K linearly for 400 ps. The systems were kept for 100 ps at 100 K. All the systems were in constant NVT ensembles using

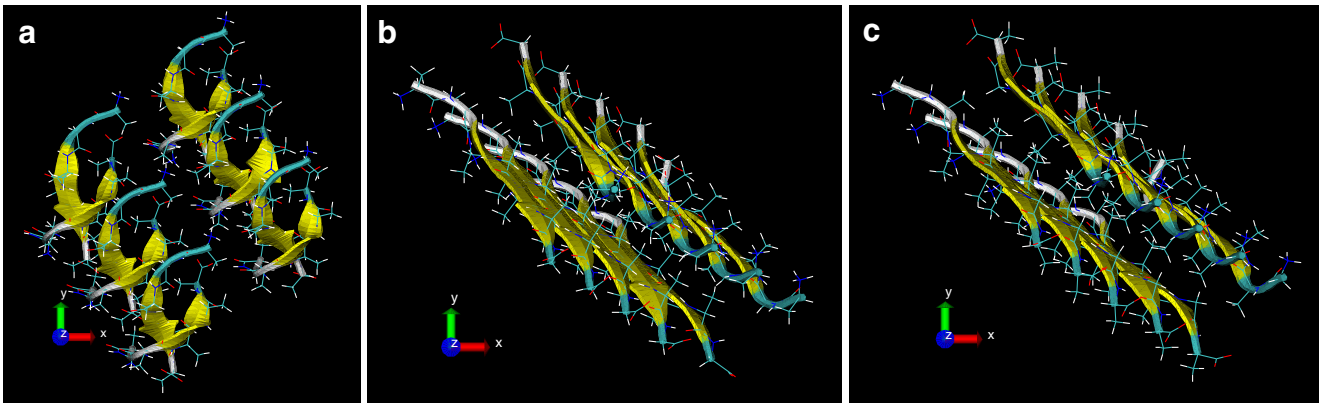

Fig. 1 Initial structures of prion AGAAAAGA amyloid fibril models 1–3

Langevin thermostat algorithm with weak restraints (a force constant of 10.0 kcal mol^{-1} $Å^{-2}$ was used) on the solvated proteins. The SHAKE and SANDER (simulated annealing with NMR-derived energy restraints) algorithms with nonbonded cutoffs of 9 Å were used during the heating, cooling and the 100 ps at 100 K. The equilibration was done in constant NPT ensembles under a Langevin thermostat for 4,400 ps and the RMSD, PRESS, and VOLUME (DENSITY) were sufficiently stable [27] for each of the models (Fig. 2); the jump in RMSD of around 0.2 Å correlates with removing restraints for the change from NVT to NPT, but it did not change the structures at

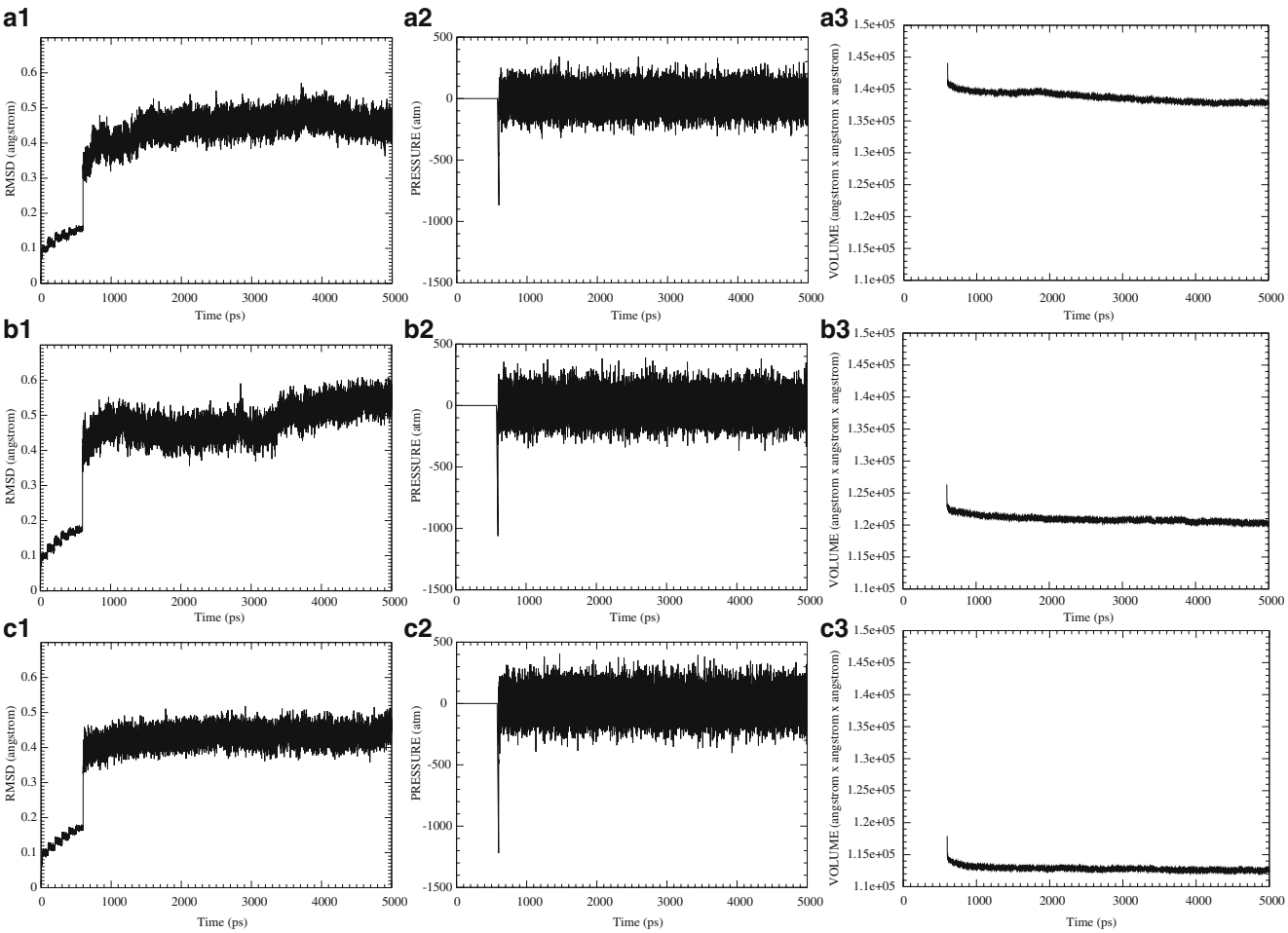

Fig. 2 RMSD, PRESSURE, and VOLUME values for Models 1–3 in 5 ns. *Upper row* Model 1, *middle row* Model 2, *lower row* Model 3

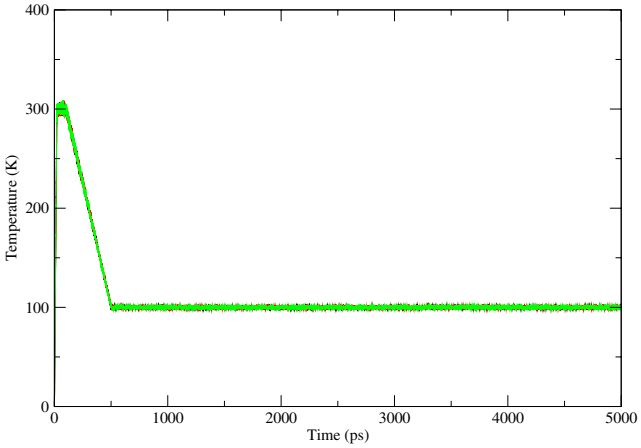

Fig. 3 Temperature-time graph of the simulated annealing (SA)

100 K. Equilibration was under constant pressure 1 atm and constant temperature (100 K) in a neutral pH environment (equilibration was performed at the low temperature of 100 K in order to be consistent with the experimental work of Sawaya et al. [19]). A step size of 2 fs was used for all SA runs. The structures were saved to file every 100 steps. During the SA, the Metropolis criterion was used. Changes in temperature with time are shown in Fig. 3.

After SA, Model 1 was refined by 10,000 steps of SD and 2,347 steps of CG; Model 2 by 10,000 steps of SD and 1,774 steps of CG; and Model 3 by 10,000 steps of SD and 619 steps of CG. All the above works were performed on the Tango facilities of the Victorian Partnership for Advanced Computing (http://www.vpac.org) of Australia. Longer simulations for the equilibration could refine the RMSD, PRESS, and VOLUME (DENSITY) values slightly further, and longer optimizations would also improve the values of ENERGY, RMS and GMAX very slightly.

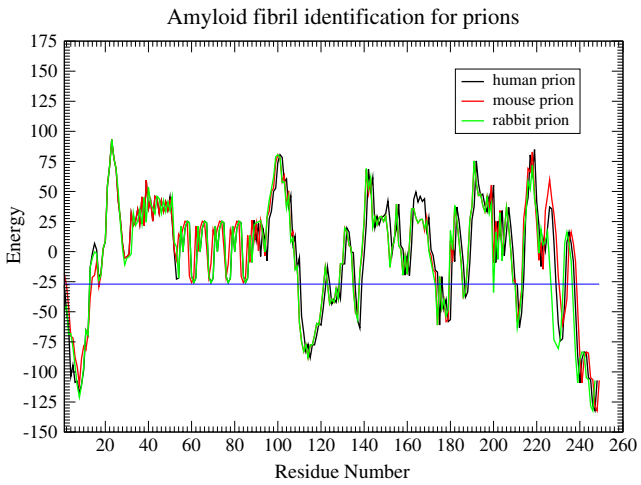

Fig. 4 Prion AGAAAAGA (113–120) is clearly identified

Results and discussion

For the sake of clarity, we use the program used by Zhang et al. [34] to theoretically confirm that prion AGAAAAGA (113–120) segment has an amyloid fibril forming property. The theoretical computation results are shown in Fig. 4, from which we can see that the prion AGAAAAGA (113–

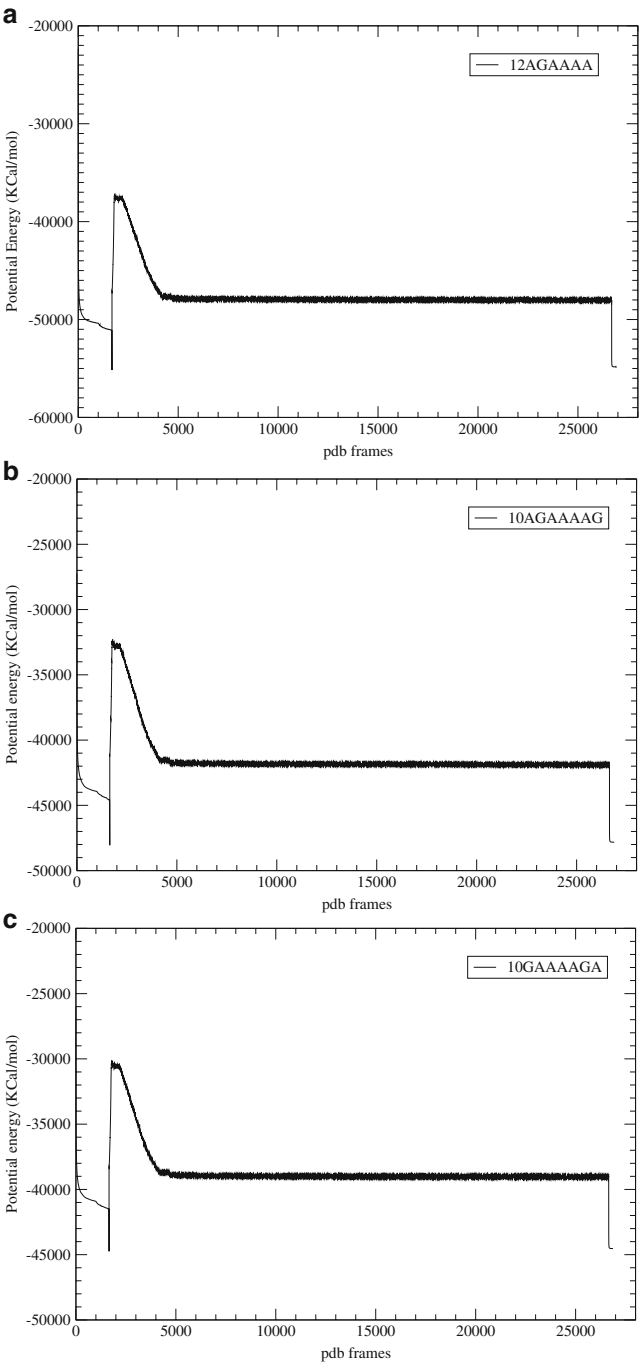

Fig. 5 Potential energy development graphs for Models 1 (*left*), 2 (*center*), and 3 (*right*)

Table 1 Potential energy values. *SA* Simulated annealing

Model	OPT1 1st step	OPT1 last step	SA 1st Step	SA last 1,000 Steps (average value)	OPT2 1st step	OPT2 last step
1	−2,233.5	−5,111.9	−55,157.8	−48,016.6	−48,027	−54,845
2	−2,725.0	−4,458.5	−48,056.1	−41,894.3	−41,896	−47,827
3	−2,603.8	−4,150.6	−44,747.5	−39,022.4	−39,049	−44,533

120) region is clearly identified as the amyloid fibril formation region because the energy is less than the amyloid fibril formation threshold energy of −26 kcal/mol [34]. In this section we will describe the optimal molecular structures of Models 1–3, firstly describing how the optimal models were obtained.

Figure 5 shows the potential energy development for the three Models. We can see that the potential energy goes down during the SD and CG optimization phase (OPT1), drops down suddenly and quickly, goes up and then slowly goes down and levels off during the SA phase (SA), and finally quickly goes down and then levels off during a short phase (OPT2). At the beginning of SA, the rapid drop off in energy is due to the temperature of the systems being changed suddenly from 100 K [19] to 0 K. This is a case of so-called "quenching". Some energy values are listed in Table 1.

In Table 1, the first column of energies (OPT1 First Step) are those derived from the LYQLEN and GNNQQNY templates by mutation. The two β-sheets are very close, with many bad van der Waals contacts, and the distance between β-strands is too short for both van der Waals contacts and hydrogen bond contacts. OPT1 removes these bad contacts, thus making the structures of the models much more stable, with lower potential energies. OPT1 makes Models 1–3 lose 2,878.4 kcal mol^{-1}, 1,733.5 kcal mol^{-1}, and 1,546.8 kcal mol^{-1} of potential energy, respectively. However, OPT1 is a local search optimization method that cannot thoroughly optimize the models into their most stable structures.

Figure 5 shows that the models are trapped in their local optimal structures. SA is a global search optimization method that can make OPT1 jump out of the local trap, even accepting very bad cases with low probability according to the Metropolis criterion. Thus, in Table 1 we see that SA rapidly quenches the molecular structures, allowing escape from the local traps; SA finally results in the loss of 7,141.2 kcal mol^{-1}, 6,161.8 kcal mol^{-1}, and 5,725.1 kcal mol^{-1} for the three systems, respectively.

After SA, OPT2 can safely bring the molecular structures of the models to the most stable states. OPT2 makes the molecules in Models 1–3 lose 6,818 kcal mol^{-1}, 5,931 kcal mol^{-1}, and 5,484 kcal mol^{-1} of potential energy, respectively. OPT2 results in a loss of energy from Models 1–3 of nearly the same magnitude as that of SA (i.e., the decrease in energy in OPT2 is significant compared to the decrease in energy in SA between the 1st step and the average of the last 1,000 steps). Compared with OPT1, OPT2 resulted in greater optimization, thus demonstrating the effectiveness of SA. The above analyses were performed for each of the three models; however, the three models are not comparable because each is independent of the others.

The final optimal molecular structures of Models 1–3 after OPT2 are shown in Fig. 6 (the RMSDs from the initial structures shown in Fig. 1 are 0.84, 1.25, 0.98 Å, respectively, for Models 1–3). The hydrogen bonds between the two closet adjacent β-strands and the van der Waals contacts between the two inner closest adjacent alanines can be seen in Fig. 6.

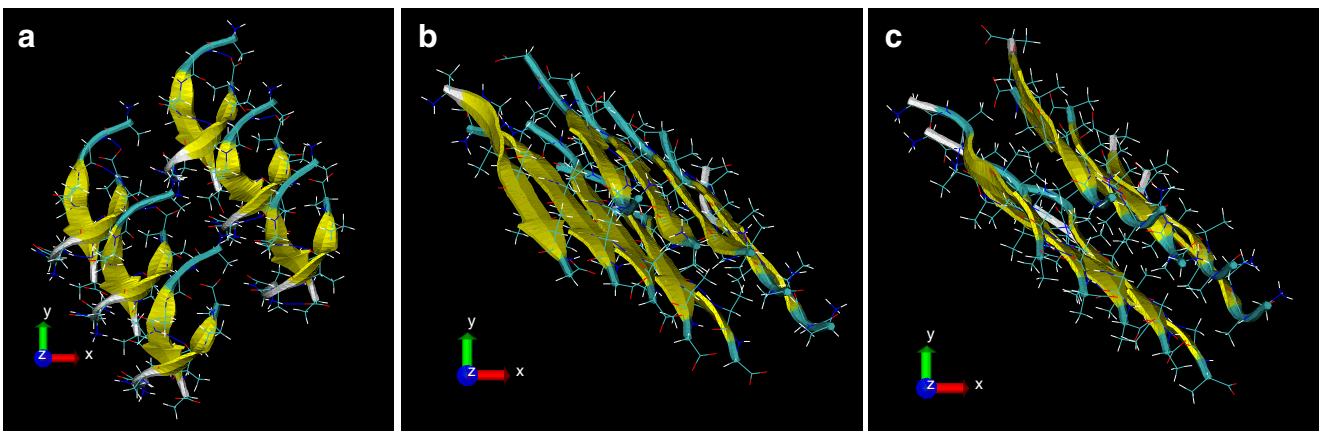

Fig. 6 Optimized prion AGAAAAGA amyloid fibril Models 1–3

Model 1 contains several hydrogen bonds in each of the antiparallel β-strands. For Models 2 and 3, in each β-sheet the β-strands are parallel to each other. It is very interesting to note that in Model 2 two chains in one sheet are tightly bonded by four hydrogen bonds, but in another sheet three chains are bonded one by one as in Model 3.

Model 1 is β-strand antiparallel, face=back, up–up [19]; Models 2 and 3 are β-strand parallel, face-to-face, up–up [19]. In all models, there is about 5 Å between the two closet adjacent β-sheets, maintained by hydrophobic bonds, and about 4.5 Å between the two closet adjacent β-strands, which are linked by hydrogen bonds. Model 1 and Models 2–3 belong to Class 7 and 1 of Sawaya et al. [19], respectively. There is a hydrophobic core in each of the models. These amyloid fibrils are rich in β-sheet structure and contain a cross-β core form of PrP^{Sc}, which causes prion diseases.

Finally, Sawaya et al. [19] proposed eight classes of steric zipper structures for peptide segments of fibril-forming proteins. For each Class, this paper constructed the molecular structures for the hydrophobic region AGAAAAGA palindrome of prion proteins (113–120). The computational numerical experience of the author allows the following statements to be made:

(1) For Class 1, based on the NNQQNY peptide from yeast prion protein Sup35 (PDB entry 1YJO), a hexamer model with six AAAAGA chains can be constructed by OPT1 but cannot pass SA and OPT2; however, based on the GNNQQNY peptide from the yeast prion protein Sup35 (PDB entry 1YJP), Model 2, with ten AGAAAAG chains, and Model 3, with ten GAAAAGA chains, were successfully constructed by OPT1-SA-OPT2;
(2) For Class 2 (i.e. β-strand parallel, face-to-back, up–up), a tetramer model with four AGAAAA chains can be constructed basing on the SNQNNF peptide of human prion 170–175 (PDB entry 2OL9) by OPT1 but cannot pass SA and OPT2;
(3) For Class 7, based on the LYQLEN peptide derived from human insulin residues 13–18 (PDB entry 2OMP), Model 1 with twelve AGAAAA chains was successfully constructed by OPT1-SA-OPT2;
(4) For other cases in Sawaya et al. [19], the β-sheet structure of prion AGAAAAGA palindrome cannot be preserved after OPT1;
(5) Based on the NNQNTF peptide of elk prion 173–178 (PDB entry 3FVA) [35–37], which belongs to Class 1 of Sawaya et al. [19], new models for the prion AGAAAAGA palindrome might be able to be constructed because six NNQNTF chains of elkPrP (173–178) are still preserved after OPT1. This will be studied further by the author.

Conclusions

To date, little structural data has been available for the hydrophobic region AGAAAAGA palindrome (113–120) of the unstructured N-terminal region (1–123) of prions. This paper reports the successful construction of three molecular structure models for the AGAAAAGA palindrome (113–120). These models should be very helpful in experimental studies on the hydrophobic region AGAAAAGA palindrome of prion proteins (113–120), for which NMR or X-ray molecular structure has not been easy to determine. This paper also shows that standard simulated annealing is a very effective tool in molecular modeling. In conclusion, this paper describes the construction of three experimentally unknown 3D structures of the hydrophobic region AGAAAAGA of prion proteins by using suitable templates from Protein Data Bank [26], with refinement of the model using several optimization techniques within AMBER. The three constructed models for amyloid fibrils may be useful in furthering the goals of medicinal chemistry.

Acknowledgments The author thanks Dr. Zhuqing Zhang (Peking University, China) for his help in preparing Fig. 4. The author appreciates the Editor-in-Chief for his suggestions and the anonymous referees for their numerous insightful comments, which have greatly improved this paper. Last, but not least, thanks go to Dr. Judy-Anne Osborn of the Australian National University and staff of Springer (http://www.springer.com/) for their help in improving my English of this paper. This paper is dedicated to the memory of my PhD supervisor Professor Alex M. Rubinov; the hybrid global and local optimization search strategy [38] of this paper was learned from him and Professor Adil M. Bagirov, another PhD supervisor of mine.

References

1. Prusiner SB (1982) Novel proteinaceous infectious particles cause scrapie. Science 216:136–144
2. Prusiner SB (1998) Prions. Proc Natl Acad Sci USA 95:13363–13383
3. Griffith JS (1967) Self-replication and scrapie. Nature 215:1043–1044
4. Brown DR (2000) Prion protein peptides: optimal toxicity and peptide blockade of toxicity. Mol Cell Neurosci 15:66–78
5. Brown DR (2001) Microglia and prion disease. Microsc Res Tech 54:71–80
6. Holscher C, Delius H, Burkle A (1998) Overexpression of nonconvertible PrP^{c} delta114–121 in scrapie-infected mouse neuroblastoma cells leads to trans-dominant inhibition of wild-type PrP^{Sc} accumulation. J Virol 72:1153–1159
7. Jobling MF, Huang X, Stewart LR, Barnham KJ, Curtain C, Volitakis I, Perugini M, White AR, Cherny RA, Masters CL, Barrow CJ, Collins SJ, Bush AI, Cappai R (2001) Copper and zinc binding modulates the aggregation and neurotoxic properties of the prion peptide PrP 106–126. Biochemistry 40:8073–8084
8. Jobling MF, Stewart LR, White AR, McLean C, Friedhuber A, Maher F, Beyreuther K, Masters CL, Barrow CJ, Collins SJ, Cappai R (1999) The hydrophobic core sequence modulates the

neurotoxic and secondary structure properties of the prion peptide 106–126. J Neurochem 73:1557–1565
9. Kuwata K, Matumoto T, Cheng H, Nagayama K, James TL, Roder H (2003) NMR-detected hydrogen exchange and molecular dynamics simulations provide structural insight into fibril formation of prion protein fragment 106–126. Proc Natl Acad Sci USA 100:14790–14795
10. Norstrom EM, Mastrianni JA (2005) The AGAAAAGA palindrome in PrP is required to generate a productive PrP^{Sc}-PrP^{C} complex that leads to prion propagation. J Biol Chem 280:27236–27243
11. Wegner C, Romer A, Schmalzbauer R, Lorenz H, Windl O, Kretzschmar HA (2002) Mutant prion protein acquires resistance to protease in mouse neuroblastoma cells. J Gen Virol 83:1237–1245
12. Brown DR, Herms J, Kretzschmar HA (1994) Mouse cortical cells lacking cellular PrP survive in culture with a neurotoxic PrP fragment. Neuroreport 5:2057–2060
13. Zhang JP (2009) Studies on the structural stability of rabbit prion probed by molecular dynamics simulations. J Biomol Struct Dyn 27:159–162
14. Cosentino U, Pitea D, Moro G, Saracino GAA, Caria P, Var RM, Colombo L, Forloni G, Tagliavini F, Salmona M (2008) The anti-fibrillogenic activity of tetracyclineson PrP 106–126: a 3D-QSAR study. J Mol Model 14:987–994
15. Henriques ST, Pattenden LK, Aguilar MI, Castanho MA (2008) PrP (106–126) does not interact with membranes under physiological conditions. Biophys J 95:1877–1889
16. Okimoto N, Yamanaka K, Suenaga A, Hata M, Hoshimo T (2003) Molecular dynamics simulations of prion proteins—effect of Ala117→Val mutation. Chem-Bio Informatics J 3:1–11
17. Villa A, Mark AE, Saracino GAA, Cosentino U, Pitea D, Moro G, Salmona M (2006) Conformational polymorphism of the PrP 106–126 peptide in different environments: a molecular dynamics study. J Phys Chem B 110:1423–1428
18. Zheng W, Wang L, Hong Y, Sha Y (2009) PrP 106–126 peptide disrupts lipid membranes influence of C-terminal amidation. Biochem Biophys Res Commun 379:298–303
19. Sawaya MR, Sambashivan S, Nelson R, Ivanova MI, Sievers SA, Apostol MI, Thompson MJ, Balbirnie M, Wiltzius JJ, McFarlane HT, Madsen A, Riekel C, Eisenberg D (2007) Atomic structures of amyloid cross-beta spines reveal varied steric zippers. Nature 447:453–457
20. Chen HF (2009) Aggregation mechanism investigation of the GIFQINS cross-β amyloid fibril. Comput Biol Chem 33:41–45
21. Lee SW, Mou Y, Lin SY, Chou FC, Tseng WH, Chen C, Lu CYD, Yu SSF, Chan JCC (2008) Steric zipper of the amyloid fibrils formed by residues 109 to 122 of the Syrian hamster prion protein. J Mol Biol 378:1142–1154
22. Simone AD, Pedone C, Vitagliano L (2008) Structure, dynamics, and stability of assemblies of the human prion fragment SNQNNF. Biochem Biophys Res Commun 366:800–806
23. Vitagliano L, Stanzione F, Simone AD, Esposito L (2009) Dynamics and stability of amyloid-like steric zipper assemblies with hydrophobic dry interfaces. Biopolymers 91:1161–1171
24. Yamaguchi K, Matsumoto T, Kuwata K (2008) Critical region for amyloid fibril formation of mouse prion protein: unusual amyloidogenic properties of the helix 2 peptide. Biochemistry 47:13242–13251
25. Zhang ZQ, Chen H, Bai HJ, Lai LH (2007) Molecular dynamics simulations on the oligomer formation process of the GNNQQNY peptide from yeast prion protein Sup35. Biophys J 93:1484–1492
26. Berman HM, Westbrook J, Feng Z, Gilliland G, Bhat TN, Weissig H, Shindyalov IN, Bourne PE (2000) The protein data bank. Nucleic Acids Res 28:235–242
27. Case DA, Darden TA, Cheatham III TE, Simmerling CL, Wang J, Duke RE, Luo R, Crowley M, Walker RC, Zhang W, Merz KM, Wang B, Hayik S, Roitberg A, Seabra G, Kolossvry I, Wong KF, Paesani F, Vanicek J, Wu X, Brozell SR, Steinbrecher T, Gohlke H, Yang L, Tan C, Mongan J, Hornak V, Cui G, Mathews DH, Seetin MG, Sagui C, Babin V, Kollman PA (2008) AMBER 10. University of California, San Francisco. Amber tutorials: http://ambermd.org/tutorials/
28. Li X, Chen XD (2005) Global convergence of shortest-residual family of conjugate gradient methods without line search. Asia-Pacific J Oper Res 22:529–538
29. Sun J, Zhang JP (2001) Global convergence of conjugate gradient methods without line Search. Ann Oper Res 103:161–173
30. Zhu H, Chen XD (2008) Global convergence of a special case of the the Dai-Yuan family without line search. Asia-Pacific J Oper Res 25:411–420
31. Bagirov AM, Zhang JP (2003) Comparative analysis of the cutting angle and simulated annealing methods in global optimization. Optimization 52:363–378
32. Kirkpatrick S, Gelatt CD, Vecchi MP (1983) Optimization by simulated annealing. Science 220:671–680
33. Humphrey W, Dalke A, Schulten K (1996) VMD—visual molecular dynamics. J Mol Graph 14:33–38
34. Zhang ZQ, Chen H, Lai LH (2007) Identification of amyloid fibril-forming segments based on structure and residue-based statistical potential. Bioinformatics 23:2218–2225
35. Gossert AD, Bonjour S, Lysek DA, Fiorito F, Wuthrich K (2005) Prion protein NMR structures of elk and of mouse/elk hybrids. Proc Natl Acad Sci USA 102:646–650
36. Gorfe AA, Caflisch A (2007) Ser170 controls the conformational multiplicity of the loop 166–175 in prion proteins: implication for conversion and species barrier. FASEB J 21:3279–3287
37. Wiltzius JJW, Landau M, Nelson R, Sawaya MR, Apostol MI, Goldschmidt L, Soriaga AB, Cascio D, Rajashankar K, Eisenberg D (2009) Molecular mechanisms for protein-encoded inheritance. Nat Struct Mol Biol 16:973–978
38. Zhang JP (2004) Derivative-free hybrid methods in global optimization and their applications, PhD thesis, The University of Ballarat, Australia